Aerodynamic and structural investigation of an active back-flow flap for dynamic stall control

S. Opitz[*], A.D. Gardner[†], K. Kaufmann[‡]

ABSTRACT

The design and experimental investigation of a back-flow flap for helicopter dynamic stall control is described. A spoiler-type flap is designed, and shown by CFD to reduce the pitching moment peak during dynamic stall by 34%. Initial experiments with a passively actuated flap in a low-speed wind tunnel showed that the opening and closing times for the flap due to the aerodynamic forces are sufficiently short and that the flap is not affected by the inertial forces of the model pitching. The experiments showed the need for a flap restraint, and that an active actuation is needed so that the flap angle is sufficient at the time of stall to have a control effect. Initial demonstrators for the structural concept of the active back-flow flap using glass-fibre reinforced polymer and a solid-state hinge are presented, showing the possibility of fabrication as an after-market add-on.

NOMENCLATURE

α	Angle of attack (°)
c	Airfoil chord (=0.300 m)
C_D	Drag coefficient
C_L	Lift coefficient; mean; peak
C_M	Pitching moment coefficient; peak
C_P	Pressure coefficient
f	Frequency (Hz)
M	Mach number
Re	Reynolds number based on the model chord
ρ_∞	Freestream flow density (kg/m^3)
t	Time (s)
v_∞	Freestream flow velocity (m/s)
ω^*	Reduced frequency: ω^*: $\omega^* = 2\pi f c / v_\infty$
x, y, z	Coordinates in flow direction, breadth and upward (m)
y^+	Dimensionless wall distance

---
[*]Corresponding Author. German Aerospace Center (DLR), Institute of Composite Structures and Adaptive Systems, Lilienthalplatz, 7 38108, Braunschweig, Germany, *Steffen.Opitz@dlr.de*
[†]DLR-Institute of Aerodynamics and Flow Technology
[‡]DLR Institute of Aerodynamics and Flow Technology

INTRODUCTION

Dynamic stall is a well-known effect for helicopter airfoils occurring when a pitching airfoil stalls, forming separated flow in a dynamic stall vortex. A lift peak and a negative spike in pitching moment form, then a rapid drop in lift appears as the stall vortex moves downstream. The torsional impulse from the pitching moment peak is a load-limiting case for the pitch links of the helicopter rotor blades. Further, high drag is experienced compared to attached flow. Dynamic stall can be controlled using passive devices, including vortex generators and changes in the leading edge contour [1, 2], but these have disadvantages at high Mach number and are limited in their control of deep stall. In contrast, active devices include actively retracting vortex generators [3], which avoid shocks at high Mach number, or air jets [4, 5], which add energy to the flow, can improve the flow control under deep stall conditions.
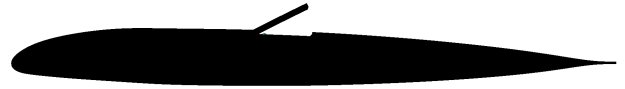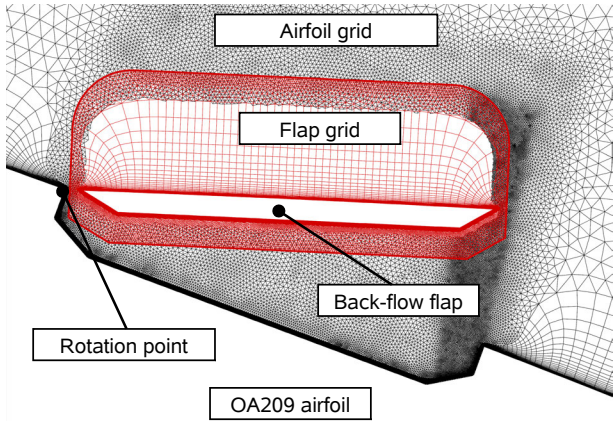

Figure 1: Back-flow flap geometry.

As part of the DLR project STELAR, alternative methods of influencing the dynamic stall using an active back-flow flap are presently being investigated [6]. The back-flow flap is a spoiler-type split-flap, attached to the suction side of an airfoil. Figure 1 shows an example of a back-flow flap. When closed, the flap lies flush on the surface of the airfoil. The flap has a hinge at its upstream end, and this can either allow flow past, or be sealed. When actuated, the angle of the flap to the airfoil increases, and reverse flow on the rear of the airfoil finds a natural limit, stopping its progression further upstream. A natural analogy is found in the feathers of birds landing, where stall is controlled by the lifting of feathers near the trailing edge of the wing.

In the past back-flow flaps have been tested on gliders by Meyer et al.[7] as a passive method of reducing stall. These freely-hinged spoiler-like flaps were located on the suction side of the airfoil near the trailing edge. When trailing edge stall occurs, the back-flow lifts the flap and the region of stall can be significantly delayed. Meyer et al. showed that a back-flow flap on the top of an airfoil near the trailing edge can increase the lift by 10-18%. Even though the effectiveness of back-flow flaps has been demonstrated in flight experiments with sailplanes, it still has to be investi-

Figure 2: Chimera grid geometry.

Figure 3: Angle of attack of the airfoil (black) and angle of the flap (red) over a pitching period.

gated whether they are also suited to improve the dynamic stall behavior of helicopter rotor blades [8].

The leading-edge stall associated with many helicopter airfoils including the OA209 [9] airfoil used for the numerical predictions, is characterized by strong backward flow along the suction side of the airfoil [10], and is different from static stall. To control dynamic stall of this type, the single dynamic stall vortex should be broken into several smaller vortices and the passage of the vortices should be delayed [11]. Initial numerical investigations with an actively actuated flap showed promising results.

NUMERICAL INVESTIGATIONS

Two-dimensional unsteady Reynolds-averaged Navier-Stokes (URANS) computations were undertaken with the DLR TAU code [12]. A dynamic stall test case with a pitching OA209 airfoil and the following parameters is carried out: M=0.14, Re=920000, ω^*=0.1, α=16±8°. Hybrid grids were created with the unstructured grid generator Centaur. A hybrid unstructured grid with triangular and rectangular elements was created with the method of Richter et. al. [13], with the boundary layer discretised using 30 rectangular layers. The relative movement between flap and airfoil used the Chimera technique [14]. This technique uses one body fixed grid for the airfoil (black) and one for the flap (red) (Figure 2). In the overlapping area the flow information is interpolated between the two grids for each time-step, requiring a strong local mesh refinement in this area. The height of the first prismatic layer and the stretching factor were adjusted to reach a y^+=1 and the boundary layer thickness, respectively. All computations were fully turbulent using the Spalart-Allmaras turbulence model [15]. The URANS computations used 1000 inner iterations and 2000 iterations per period as [13]. After two pitching cycles, convergence was reached assuming a maximum difference of 1.5% between the lift coefficient of the second and third period.

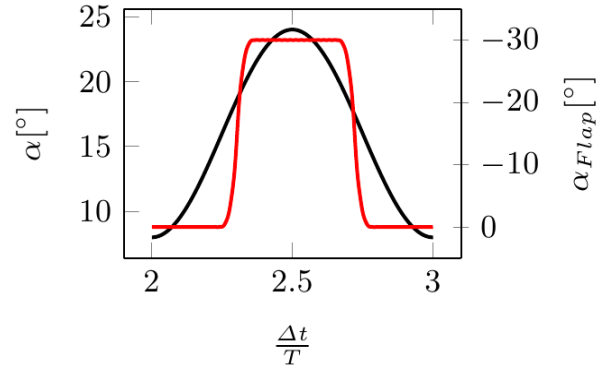The flap actuation was designed to be a square-wave with rounded corners, so that the flap would be fully open at the moment of leading edge stall, and closed during the separated flow. Figure 3 shows the flap actuation strategy with an open flap only at high angles of attack. Several flap actuation strategies were investigated [16], and this was found to be a good compromise between realizable actuation speeds and correct timing of the flap actuation.

Figure 4 shows a comparison between the flow during dynamic stall for M=0.14, Re=920000, ω^*=$2\pi fc/v_\infty$=0.1, α=16±8°, at α=21° on the upstroke, during the primary peak in pitching moment caused by the dynamic stall with and without flap actuation. In both cases, a large dynamic stall vortex is formed, with an associated low pressure region, which causes both an overshoot in lift, and an increasing pitching moment as the vortex travels towards the trailing edge of the airfoil, as the moment arm increases. The distance between the dynamic stall vortex and the airfoil increases as it moves downstream, decreasing the force due to the region of low pressure, and thus the instant of both maximum lift and minimum pitching moment is usually before the vortex reaches the trailing edge of the airfoil [17]. The flap is dynamically actuated to only be deployed during the stalled flow, and this is the test case found by Kaufmann [16] as the best flap position and actuation prescription studied. The flap actuation starts well before stall, so that at the point of stall the flap is in a position to act on the separated flow. It can be seen in Figure 4 that the back-flow flap breaks the main stall vortex into smaller structures, and reduces the strength of the pressure minimum contained in the largest vortex. The total size of the separated region is smaller, resulting in less diversion of the flow over the airfoil, and increasing the lift on the airfoil.

Figure 5 shows a comparison between the lift and pitching moment for the airfoil with and without flap actuation. The start of flap actuation at around α=18° is visible as a bump in the lift in Fig. 5 (Left), and the case with flap actuation starts the lift peak of stall at the same time as without flap actuation. The overshoot in lift is reduced with flap actuation, and the second lift peak seen without actuation does not appear. After stall the lift is similar between the two configurations, and the flap closing around α=17° on
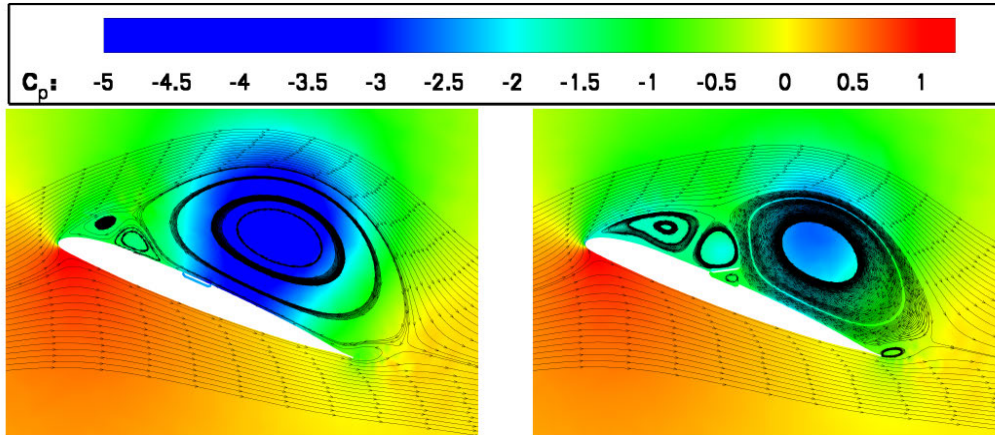
Figure 4: Comparison of streamlines and pressure for flow without flap actuation (Left) and with flap actuation (Right) for the OA209 airfoil at M=0.14, Re=920000, ω^*=0.1, α=16±8°, at α=21° on the upstroke.
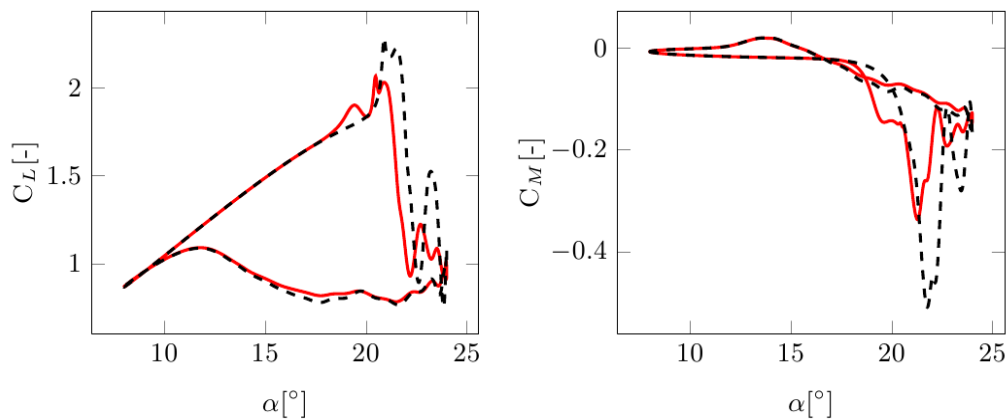

Figure 5: Comparison of lift (Left) and pitching moment coefficient (Right) for the OA209 airfoil at M=0.14, Re=920000, ω^*=0.1, α=16±8°. The black lines are without flap actuation, and the red lines are with flap actuation.

the downstroke is not clearly visible in the lift. The reattachment of the flow is at around α=10° on the downstroke, regardless of the flap actuation.

The pitching moment in Fig. 5 (Right) shows an early excursion to negative pitching moment as the flap is actuated, but during the main stall a reduction in the pitching moment peak of 34% compared to the reference case without actuation is observed. As for the lift, the second peak in the pitching moment does not appear when the flap is actuated, and the pitching moments after stall are similar between the cases with and without flap actuation.

EXPERIMENT WITH A PASSIVELY ACTUATED FLAP

The initial numerical study was done using an actively actuated flap, with a small gap between flap and airfoil, as this was the simplest configuration to use numerically. This investigation left several open questions:

- What is the effect of the true flap geometry, with sealed leading edge?
- Will the passive actuation of the flap through the backflow after separation be sufficient to open it?
- For attached flow, is the flow sufficient to hold the flap closed against the inertial forces of the model pitching?

To investigate these questions, an initial experiment was performed in the 1MG low speed wind tunnel in Göttingen. This tunnel has an open test section of 1 m width and 0.70 m height and flow at 50 m/s was used on a NACA0012 airfoil of 0.3 m chord, pitching at α=20±8° and f=3-6 Hz: the same conditions as in the CFD above, but with the mean angle increased to compensate for the large blockage of this wind tunnel model. As seen in Figure 6, the flap was attached to the suction side of the model with tape, and the deployment of the flap was restrained in angle using cords. The flow was monitored using tufts and a high-speed video camera, with which the flap deployment and flow direction on the suction surface were monitored. For this experiment

the model pressures were not monitored. In Figure 6, the model is at high static angle of attack, and the flow on the airfoil is separated. This static separated flow causes a reverse flow on the suction side of the airfoil, which lifts the flap from the surface of the airfoil. The flap angle is restrained by cords, meaning that the opening angle remains constant at the maximum possible angle of attack. Tests without the flap restrained showed that the flap had a continuous unconstrained motion, which depended on the flow condition. In the worst case, the flap increased in angle until it was reversed along the airfoil, after which it fully returned to the closed position, leading to a wildly unsteady flapping motion.

Figure 6: Passive back-flow flap model in the 1MG at 50 m/s. Flow is from left to right.

As shown for computational results on a clean OA209 airfoil in Figure 7, the pressure along the suction side of the airfoil increases monotonically toward the trailing edge. When the flap is on the surface of the airfoil, the pressure under the flap is (roughly) that at the trailing edge of the flap. Since the pressure increases from the front to the back of the flap, this results in a higher pressure under the flap than on top of it, and the flap angle increases. As the flap angle increases, the pressure on the top of the flap increases, and this allows the flap angle to stabilize at a minimum angle of around 5-10° to the surface, depending on the flap position. Perforating the flap resulted in a reduction of this angle, but the results were still unsatisfactory for the surface quality required for normal flight. An extreme example of the effect of a pressure gradient on the flap could be observed by positioning the flap in or close to the suction peak, which resulted in stabilised angles of around 45°, thus having the flap fully opening even when no separated flow was present.

The analysis of the high-speed videos (Fig. 8) showed that the back-flow flap self-actuated due to the back-flow of the dynamic stall vortex. This video was taken with a hand-held camera at 120 frames per second, and thus the interframing time is 8.33 ms. Figure 8(a) shows the top of the airfoil during pitch-up just before stall. The flow is
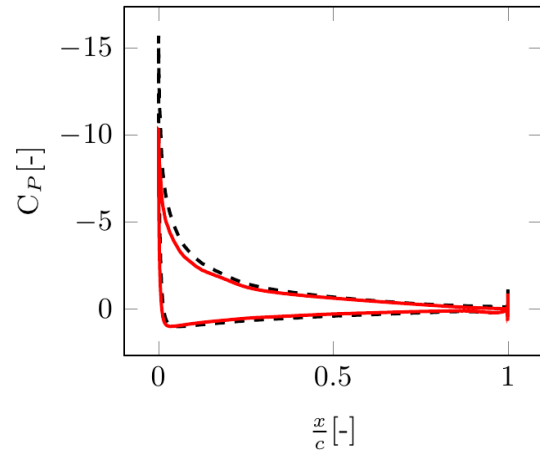

Figure 7: Pressure distribution on the OA209 airfoil with no flap at M=0.14, Re=920000 via CFD. Red: Steady 14 Black: Unsteady 18, upstroke.

fully attached, and the flap is lying flat on the surface of the airfoil. Directly behind the flap some tufts are reversed, since there is a small separation on the surface here, due to the residual flap angle in attached flow. In this case, the flap is a strip of 0.5 mm thickness aluminium, with length 30 mm (x/c=0.10). The leading edge of the flap is secured by a length of tape at x/c=0.52, and this is also the hinge point. Due to the tape, there is no flow through the hinge point. Figure 8(b) shows that the flow is fully separated on the top of the airfoil from around 10% chord , with the time for flow separation being around 25 ms. The reverse flow is fully established, but the flap has just started to move away from the static position on the airfoil which it held for attached flow. Although the flap started to actuate immediately after the airfoil stall, it was not fully actuated for around 0.025 seconds. Figure 8(c) shows the flap that has reached the position where it is restrained from opening further by the cords. At this pitching condition, this delay is equivalent to a change in angle of attack of $\Delta\alpha$=5°. If the flap were actuated early enough, this would be a sufficiently short actuation time, but the actuation only starts after the flow separation, and thus the flap is always too late to control the dynamic stall vortex. This suggests that an active flap would be necessary.

If the flap was not restrained by the cords, the back-flow resulted in the flap being completely flipped, until it lay backward on the airfoil surface. Thus a restraining mechanism to limit the flap maximum angle is necessary. Figure 8(d) shows the start of flow reattachment. For this airfoil the flow reattached starting at the leading edge, and in Fig. 8(d) the tufts at the leading edge of the airfoil are in the direction of flow, indicating attached flow, while the rest of the tufts still indicate separated flow. At this point the flap starts to close simultaneously with the reattachment of the flow. In Figure 8(e), 17 ms after the start of flow attachment, the flap is fully closed, and the flow downstream of the flap can start to reattach. One camera frame later, in Figure 8(f), the flow was fully attached. The flap self-
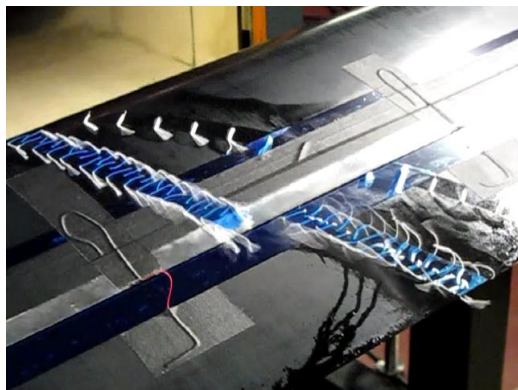
(a) *t*=0, attached flow
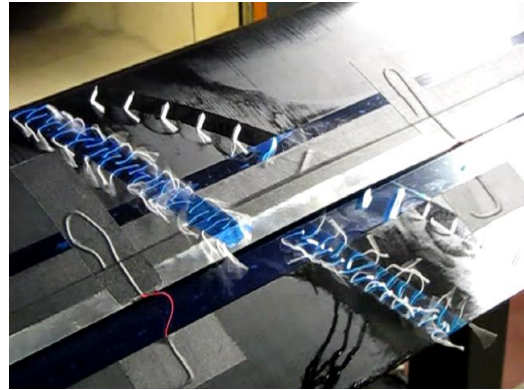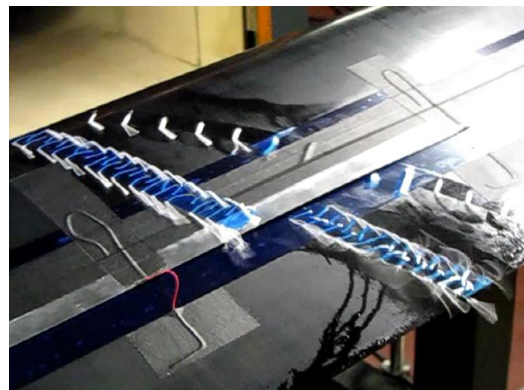

(b) *t*=25 ms, separated flow, flap closed

(c) *t*=50 ms, separated flow, flap open

(d) *t*=108 ms, flow attached on LE, flap open

(e) *t*=125 ms, flow attached to flap, flap closed

(f) *t*=133 ms, attached flow, flap closed

Figure 8: High-speed video frames of the pitching experiment α=20$\pm$8° at f=6 Hz, with a flap of length x/c=0.10, with hinge at x/c=0.52, constructed of aluminium plate of thickness 0.5 mm.

closed in acceptable time as the flow reattached.

The use of different materials to vary the weight and inertia of the flap (thick flap of brass, thin flap of aluminium), showed that the aerodynamic forces were much larger than the inertial forces (Fig. 9). The pressure distribution from the attached flow counteracted the inertial forces due to pitching, at pitching frequencies of up to $f = 6Hz$, keeping the flap close to the model surface during attached flow. Unfortunately, as for the static flow, the pressure gradient over the flap during attached flow caused it to not lie perfectly flat on the airfoil surface, but to stabilize at a minimum angle of around 5-10° to the surface, depending on the flap position. The conclusion was thus that the back-flow flap should have active actuation to open during stall, and active actuation to hold it closed during attached flow.
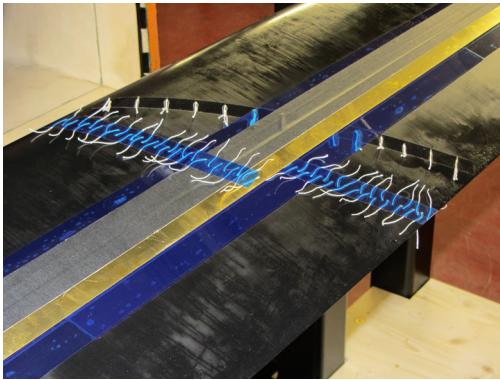

(a) Flap closed

(b) Flap deployed

Figure 10: First structural demonstrator for a GFRP back-flow flap "glove" with solid state hinge and angle restraint.

Figure 9: Flap of 0.6 mm brass for the investigation of effect of flap inertia.

STRUCTURAL DESIGN OF THE FLAP

Motivated by the first numerical predictions and the initial wind tunnel experiments the structural realization of such a flap was investigated. Ideally it should be possible to retrofit the back-flow flap to existing blades. Numerical investigations showed that attaching the hinge and flap as a "bump" on the top of the airfoil always resulted in an unacceptable increase in drag (particularly at high Mach number), regardless of the flap geometry. Therefore a concept to fit the whole system into a "glove" of thickness 5mm, to be attached to the upper side of the rotor blade airfoil was pursued. This restriction on the available space for the flap and actuator is challenging, but realizable. In contrast to the initial experiments, the back-flow flap should be integrated into the blade surface without steps or gaps. Furthermore, the hinge that connects the flap to the blade should be robust enough to enable a reliable deployment at high frequencies without significant friction or wear within the strong centrifugal field of a helicopter rotor. Using composite materials for the flap offers the possibility of integrating functionalities like an actuator or a hinge directly into the structure [18, 19].

A prerequisite for the integration of these functionalities during the manufacturing process of the composite is the selection of compatible raw materials. For the presented back-flow flap a GFRP-prepreg was used for the main structure of the "glove". The matrix is cured at 120°C. The elastomeric material used for the solid state hinge and for the angle restraint is customized so that it can be vulcanized at the same temperature. This finally allows the combination of cure and vulcanization in one process. Consequently a relatively strong adhesion between both materials can be obtained. As usual for composites the different materials are placed layer by layer on a mould. Here a negative mould was used to guarantee that the outer contour of the airfoil is matched. Numerous separating foils are used to assure that the flap and the angle restraints are only connected in predefined areas which enables the flap to lift after cure. Due to the integral design and manufacturing concept the glove with solid state hinge and angle restraint can be manufactured in one shot. Figure 10 gives an impression of how the structurally integrated solid state hinge connects the GFRP-flap to the "glove" that is used to retrofit the back-flow flap to an existing blade.

Within this paper two different actuation mechanisms will be presented and evaluated, both of which have the potential to operate under the adverse conditions of a helicopter rotor. The first is based on a piezoelectric actuator [20, 18] that is able to bend the back-flow flap and therefore to support the self-actuation of the flap. The second relies on magnetic forces for the deployment of the flap. Both

concepts take advantage of integration of the actuator into a back-flow flap that is made of GFRP.

SOLID STATE HINGE

The surface of the hinge that connects the flap to the blade should be as smooth as possible to prevent any disturbance of the flow when the flap is not deployed. For this reason conventional hinges, consisting of two hinge leaves, are not suited. Further, those joints rely on the relative movement of two solid bodies. Even though lubricants can reduce the amount of friction produced in the contact area between both hinge leaves, high frequency actuation would cause significant wear. For the application on a real helicopter blade the centrifugal forces would make all problems arising with friction and wear even more severe. All these issues can be addressed using a solid state hinge. Solid state hinges generate the relative movement of the rigid parts by elastic deformation of a flexible region. Since they have no moving parts they do not suffer from friction or wear. Figure 11 depicts the general design and dimensions of the solid state hinge that connects the flap to the blade.
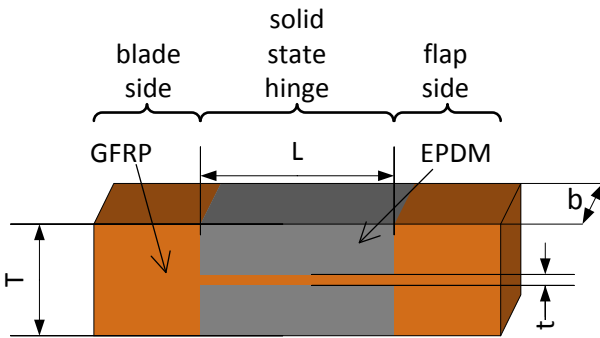

Figure 11: Principle and dimensions of solid state hinge.

The material in the flexible region must sustain the strains occurring without any plastic deformation. Nevertheless it should have a certain stiffness to prevent large longitudinal strains. As GFRP (Glass Fibre Reinforced Polymer) shows a linear elastic material behavior up to large strains it is a well suited material for this application. Since the fracture strain in fiber direction of a unidirectional GFRP material is higher than transverse to the fiber, the fibers should be oriented in parallel to the neutral axis of the hinge. In this configuration, bending of the hinge does not produce a coupled torsion deformation. In principle the strains due to bending remain small as long as the material is located close to the neutral axis. However due to manufacturing constraints the thickness t of the flexible part of the hinge can not be arbitrarily small. The hinge is designed to have a symmetric three layer setup. The middle layer GFRP directly connects the flap to the blade. As this thin layer would be quite fragile, it is encapsulated in EPDM (Ethylene Propylene Diene Monomer). The larger distance of the elastomer to the neutral axis, results in bigger strains in the EPDM layers. But as this highly flexible

material can easily bear strains of 100% and more, EPDM is an excellent material for this application.

As the degree of freedom in a solid state hinge is realized through an elastic deformation, the joint is always characterized by a certain spring characteristic. Consequently an additional force or moment has to be overcome to deploy the flap. For the design process the knowledge of the elastic characteristic of the hinge is needed. For this purpose a simple and fast analytical model to predict the bending stiffness of the 3 layer setup was verified with numerical investigations and finally validated with experimental data. For the analytical prediction of the spring characteristic the bending stiffness of the solid state hinge is linearly proportional to the extruded length of the hinge b. For the calculation of the equivalent torsional spring characteristic c_t, textbook formulas can be used [21]. The inclination angle α at the end of a uniform beam with the length L and the bending stiffness EI_{SSH} that is deformed by a bending moment M at the free end can be calculated by:

$$\alpha = \frac{M \cdot L}{EI_{SSH}} \tag{1}$$

$$c_t = \frac{M}{\alpha} \tag{2}$$

$$\frac{c_t}{b} = \frac{EI_{SSH}}{b \cdot L}. \tag{3}$$

In order to verify and validate the analytical estimation of the spring characteristic 4 different configurations of solid state hinges were investigated. A summary of the different designs is given in Table 1.

Table 1: Solid state hinge configurations.

config.	t [mm]	T [mm]	L [mm]	comment
1	0.125	1.125	10	50% cut out
2	0.125	1.125	10	-
3	0.125	1.125	15	-
4	0.25	1.25	10	-

To adjust the stiffness of the hinge, different design variables can be used. The configurations investigated comprise 2 different thicknesses of the central GFRP layer t as well as 2 length of the hinges L. As the GFRP-layer could not be further reduced in thickness (due to manufacturing constraints), configuration 1 had cut outs in the direction of the extruded length b. Consequently only 50% of the hinge area was covered with GFRP. The cut outs were filled with EPDM to prevent any holes allowing pressure equalization between the upper and the lower flap surface. In the analytical and numerical prediction this modification was modeled via a reduction of the elastic modulus of the middle layer according to a simple rule of mixture. Finally all four configurations were manufactured. For the experimental determination of the spring constant c_t a universal testing machine was used. The machine was equipped with a 10 N load cell. The load cell was connected to the flap by a thin sting in such a manner that the movement of the tra-

verse of the testing machine opened the flap while the load cell measured the corresponding string force. The opening angle of the flap as well as the angle between the flap surface and the force were captured in equidistant steps of the traverse position. Therefore a photograph, taken for each step, is post-processed via image processing software. Finally the force component orthogonal to the flap surface is used to calculate the moment at the middle of the solid state hinge. The spring constant is then determined as the linear coefficient between flap angle and moment.
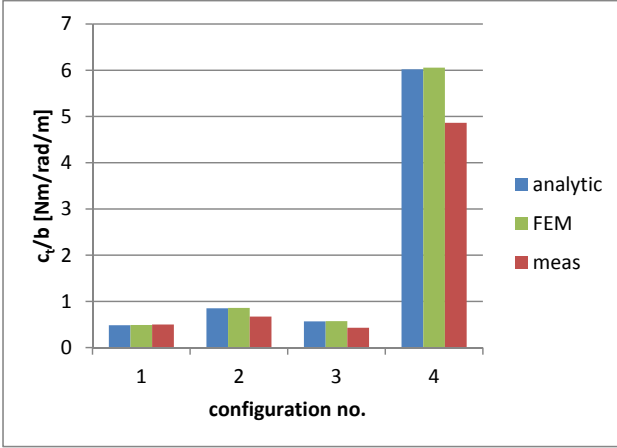

Figure 12: Comparison of torsional stiffness.

Figure 12 shows the comparison between the analytical and numerical prediction of the spring characteristic and the measured values. While the numerical (FEM) and analytical results (analytic) are in very good agreement (deviation less than 1.5%), the measured values (meas) only reproduce the trend of the prediction. The deviations are up to 25%. Analysis of the contributions of GFRP and EPDM to the total bending stiffness of the hinge showed that the GFRP delivers the major contribution to the bending stiffness as its Young's modulus is about 4500 times higher. For the investigated designs only one or two layers of GFRP-prepreg (pre-impregnated fibers) are used. The resulting layer thickness is approx. 1/8 mm. Due to manufacturing and material deviations this thickness can not be guaranteed. Micrographs of the manufactured hinges indicated deviations in thickness of a few 100th of a millimeter. Changing the single layer thickness in the analytical and numerical prediction by only 1/100 mm can bring the deviations down to less than 6%. Consequently the analytical and the numerical model can be evaluated as sufficiently accurate with respect to the achievable manufacturing accuracy.

To calculate the opening force as a function of the flap angle the kinematics of the flap has to be regarded, as shown in Figure 13. Assuming a constant mean moment over the length of the solid state hinge the relative motion of the flap can be described as follows.

$$r = \frac{L_{EPDM}}{\alpha} \qquad (4)$$

$$v_0 = v(x=0) = r \cdot sin(\alpha) - L_{EPDM} \qquad (5)$$
$$w_0 = w(x=0) = r - r \cdot cos(\alpha) \qquad (6)$$
$$w(x) = w_0 + x \cdot cos(\alpha) \cdot tan(\alpha) \qquad (7)$$
$$v(x) = v_0 + x \cdot cos(\alpha). \qquad (8)$$

For a given position x of the center of force of an actuator, the motion with respect to the flap angle can be calculated. This kinematic relation was used for the finite element simulation to predict the moment at the solid state hinge generated by the actuators according to the flap angle.
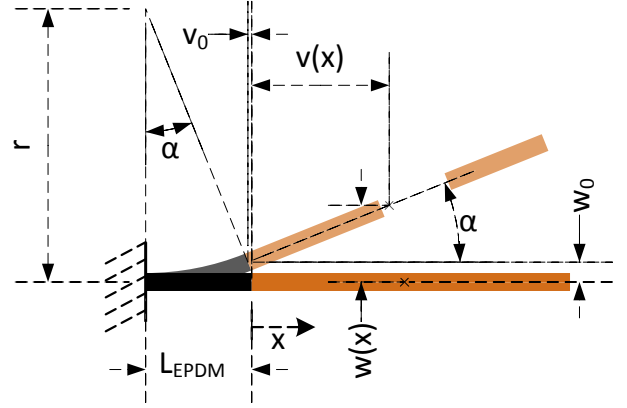

Figure 13: Kinematics of the back-flow flap.

ANGLE RESTRICTION

One outcome of the initial wind tunnel experiments was that a restriction in the opening angle of the flap is needed. Without a limit in the flap opening angle the highly dynamic process caused the flap to flip over. The spring characteristic of the solid state hinge can only partially improve this behavior. A drawback of the solid state hinge concept is that it is not possible to use a catch like those available for conventional hinges. The basic idea is to limit the flap angle in a similar manner as already done in the wind tunnel experiments. There a cord was attached to the flap as well as to the blade surface. When the flap opened this string was put under tension and limited the opening angle. This worked for the initial tests but showed significant wear already after a short measurement time. Furthermore the strings were in the flow when the flap was not deployed. This increases the drag and can possibly disturb the natural flow. Consequently a robust restraining mechanism that is integrated into the "glove" and does not disturb the flow is needed. Figure 14 shows the basic idea how the angle restraint for the flap with the solid state hinge can be realized.

The restraint mechanism is located underneath the flap in such a manner that the outer surface remains totally smooth if the flap is not deployed. In contrast to the wind tunnel experiments the catch is now a strip that has a certain width in the direction of extrusion (b), matched to the loads, and is no longer a cord. This also guarantees that the strip is always in the same position when the flap is closed. The
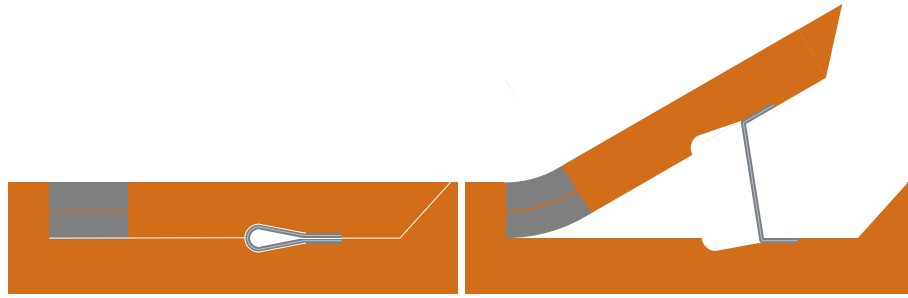
Figure 14: Principle of flap with solid state hinge and angle restraint (Left: closed, Right: opened).

maximum opening angle can be set by the proper position and length of the strip. The strip should have almost no bending stiffness but should not elongate significantly to limit the deployment angle to a certain value. A three layer setup of EPDM and glass fibers is identified as an ideal material combination for the strip. Compared to the solid state hinge the bending stiffness of the strip was significantly reduced, since an actuator has to overcome this additional stiffness to deploy the flap. For this reason the GFRP material used for the middle layer of the solid state hinge was replaced by a very thin glass fiber fabric (50 g/m^2) that was not impregnated with epoxy resin so that the elastomer directly embeds the glass fibers in the strip. To reduce the thickness of the strip in stored condition the thickness of the EPDM layers was also decreased. To identify the ideal way to connect the strip, the peel off force between strip and GFRP for different configurations was determined by a customized test in a testing machine.

ACTUATION MECHANISMS

For a reliable operation of the flap an actuation mechanism is needed. For the investigation of the aerodynamic effect the ideal solution would be an actuator that can directly control the flap deployment angle in the same way as the angle was set during the simulation. Unfortunately such an actuator would have to be quite powerful and once again the limitation in mounting space excludes a lot of the technologically possible solutions. As a compromise between an easy to realize passive flap and a fully active deployable flap the goal is here to develop an actuator that can support the self deployment of the flap by the flow. Such a concept is more likely to be fitted into the "glove". Furthermore the efficient use of system inherent forces will result in quite low energy consumption of the actuation system. In this section of the paper two different approaches for actuation mechanisms that can initiate a flap deployment by the flow are presented and assessed.

BENDING ACTUATOR

Composite materials allow the integration of different kinds of actuators directly into the structure. In the past mainly piezoelectric actuators were used. Since the strain

of those actuators is the response to an electric field, they are easy to operate. The piezo-ceramics introduce strain into the structure which leads to the desired morphing. Further, these materials have already proven that they can be operated in the centrifugal field of a helicopter rotor [22, 19]. Different types of piezoelectric actuators are available. For the integration into the back-flow flap "glove" especially thin piezo-composite actuators are of interest [23, 20]. They require only a very limited mounting space and can be integrated even in curved composite parts [24]. The intended operation principle was to integrate a piezo-composite actuator directly into the flap (see Figure 15). The actuator should not be located in the neutral axis of the flap laminate. Consequently the generated strain (see Figure 15, Middle, red arrow) causes a bending of the flap. This deformation would be used to lift the trailing edge of the flap from the blade surface. The back-flow which develops on the airfoil surface should open the flap.

The crucial point of this concept is the assessment of whether the performance of the bending actuator is sufficient to produce a significant flap bending. For the analytical assessment of the bending performance of the integrated actuator, three steps are required.

1. position of neutral axis of the layered setup (fibre composite, piezo-composite)
2. bending stiffness of the setup
3. actuator moment

Using an analytical tool based on fundamental mechanics different designs were evaluated. The study comprised configurations with one and two piezo-composite actuators (2 or 3 layer setup) and various flap thicknesses and materials. The displacement at the trailing edge of the flap was calculated without any forces from the flow. It can be summarized that the maximum displacement for a flap with a length of 40mm did not exceed 1mm. This relatively small displacement in combination with the experiences from initial wind tunnel experiments led to the conclusion that the risk of insufficient actuation authority is too high to further pursue this actuation concept. A second deficit that confirmed this decision is the fact that this actuator is not able to keep the flap closed during attached flow. Consequently alternative actuation mechanisms are investigated.
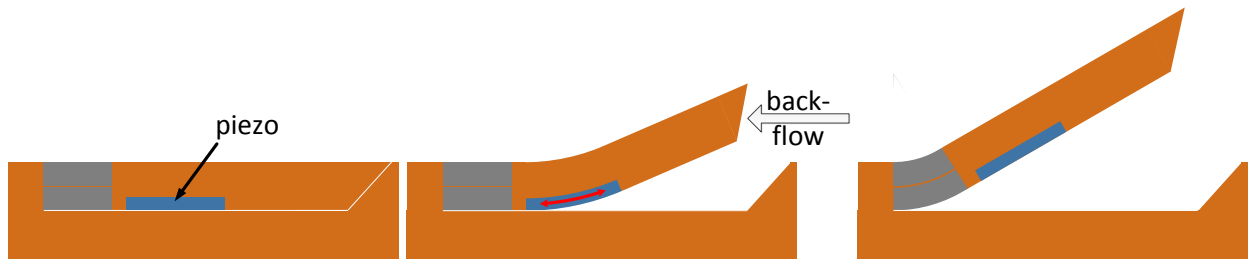
Figure 15: Principle of flap with piezoelectric bending actuator (Left: closed, Middle: actuator induced bending of the flap, Right: flap fully opened by back-flow).

PERMANENT MAGNET

A quite simple approach is the deployment of the flap with two permanent magnets. As those can not be switched on and off, it is necessary to move one of the magnets. The zero energy requirement to keep the flap closed when not needed make permanent magnets an attractive option. The basic principle of operation and the orientation of the magnets can be seen in Figure 16.
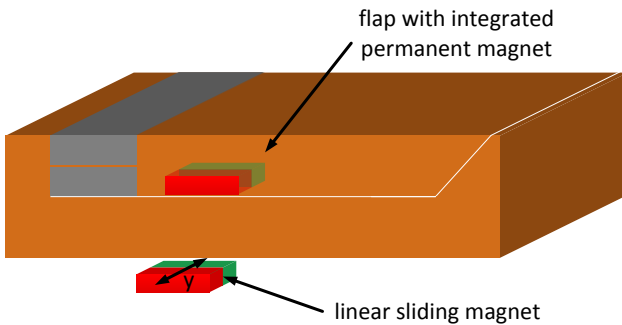

Figure 16: Principle of flap with integrated permanent magnet.

While one neodymium magnet is integrated in the flap during the manufacturing process, the second one can be linearly slid underneath the flap. This motion could be generated by an electromagnet and a push rod at the root of the blade but the detailed design of this mechanism is not the focus of this work. Increasing the number of magnet pairs also increases the force that deploys the flap. In order to predict the forces between the two magnets static finite element calculations were performed. Since the remanent magnetization of the neodymium magnets used is only roughly known the calculations are accompanied by an experimental characterization. The tests were performed in a universal testing machine (see Figure 17). Each of the neodymium magnets was glued to a CFRP (Carbon Fibre Reinforced Polymer) plate in order to have a sufficient distance to all ferromagnetic parts of the machine that could influence the measurement. To characterize the interaction of the two magnets the force in z-direction as a function of Δz was captured for different lateral offsets Δy. As the setup was rather stiff and the range of measured force is low compared to the measurement range of the testing machine, the position of the transverse was used to calculate the gap
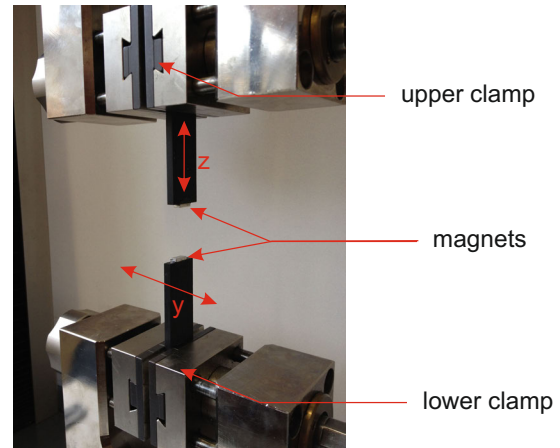

Figure 17: Setup for the characterization of neodymium magnets.

Δz between the magnets. Furthermore any lateral bending of the CFRP-plates was neglected. Hence the value set for the lateral distance Δy is assumed to stay constant during each measurement. In parallel to the experiment the setup was modeled using the finite element method. To set the remanent magnetization the geometric setup for the point of maximum force within the measurements ($\Delta y = 0$, $\Delta z = 0.5mm$) was simulated. At this position the magnetization was varied to match the measured value. Once this value was set, it remained unchanged for all further computations with varying values for Δy and Δz. Figure 18 depicts the comparison between the measured and the computed characteristics of the magnets.

Looking at these results the following conclusions can be made. The measured results and the finite element prediction are in good agreement. The magnets can generate a maximum force of almost $5\,\mathrm{N}$ which is quite remarkable for the investigated magnets that have a size of $4.5\,\mathrm{mm} \times 10\,\mathrm{mm} \times 2\,\mathrm{mm}$ and a weight of $0.7\,\mathrm{g}$. As expected the force rapidly drops when the gap between the magnets gets bigger. There is a small region of lateral distance where the increase of the gap Δz first leads to a slight increase in force until the force drops again. If the lateral distance between the magnets gets big enough they attract each other. The latter effect can be used to keep the flap closed during attached flow. The finite element computa-
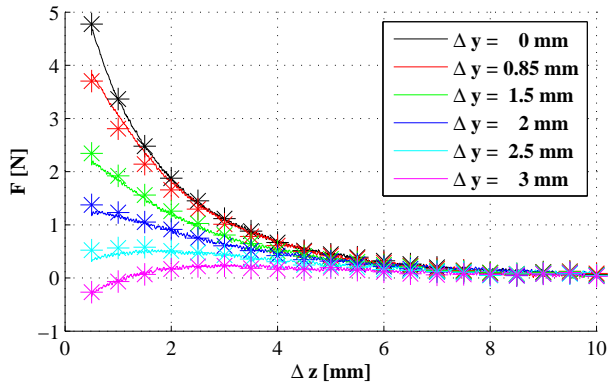
Figure 18: Results of characterization of neodymium magnets. Lines depict measured values and symbols FEM values.

This paper presents a structural design concept for a back-flow flap. The development was encouraged by the predicted benefits of initial numerical investigations, which showed that with active actuation of a back-flow flap at Mach 0.14, the pitching moment peak could be reduced by 34%. Initial wind tunnel experiments were performed and showed that although the flap actuation time due to the aerodynamic forces was acceptably short, that it actuated too late to control stall. Further, the flap needs to be held closed during attached flow, since the pressure gradient on the rotor blade airfoil causes the flap not to lie flush with the surface. The necessity for an angle restriction to control the unsteady motion of the flap was identified.

The attachment of the flap via a structurally integrated solid state hinge and an angle restriction mechanism were presented to fulfill these requirements, and a demonstrator with integrated hinge and flap in a "glove" to be mounted on an existing rotor blade was presented. Two different actuation concepts were investigated and assessed. It could be shown that a bending actuator that is integrated into the flap does not have enough authority to initiate a reliable deployment of the flap. The combination of two permanent magnets seems to be more promising, with sufficient strength to actuate the flap and to keep it closed during attached flow. The zero energy requirement to keep the flap closed when not needed make permanent magnets an attractive option.

After the manufacturing of the wind tunnel model a final test campaign will show the effectiveness of the system under wind tunnel conditions. The challenges that arise under rotating conditions were not in the focus of this paper but had to be kept in mind. After further aerodynamic simulations have identified the radial location of such a flap the transfer of the presented wind tunnel technology to a rotor will be investigated.

tions in Figure 19 show that sufficient attractive and repulsive forces to overcome elastic and aerodynamic forces can be obtained by varying the actuator magnet position in the lateral direction. The maximum attraction force F_z occurs at a lateral offset of Δy=4.5 mm and has a magnitude of approx. 2 N.
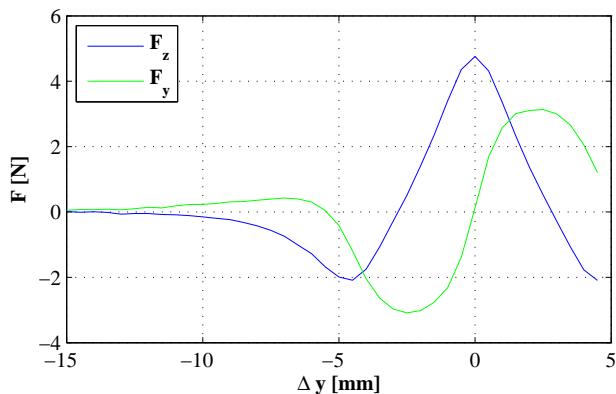

Figure 19: Prediction of z and y force as a function of lateral offset Δy for constant Δz=0.5 mm.

The tools presented so far can be used to investigate further concepts for a magnetic actuation. The design using 2 permanent magnets can serve as benchmark in terms of actuator performance. As it is advantageous to have as few moving components as possible in the centrifugal field of a helicopter rotor, it is self-evident that it would be beneficial to replace the moving magnet by an electromagnet. The challenge is to design the electromagnet that is strong enough to have a comparable performance as the neodymium magnet used so far and that fits into the slim "glove" of the back-flow flap. Concepts using electromagnets will be investigated in future work.

Copyright Statement

The authors confirm that they, and/or their company or organization, hold copyright on all of the original material included in this paper. The authors also confirm that they have obtained permission, from the copyright holder of any third party material included in this paper, to publish it as part of their paper. The authors confirm that they give permission, or have obtained permission from the copyright holder of this paper, for the publication and distribution of this paper as part of the ERF2013 proceedings or as individual offprints from the proceedings and for inclusion in a freely accessible web-based repository.

References

[1] Mai, H., Dietz, G., Geissler, W., Richter, K., Bosbach, J., Richard, H., de Groot, K., "Dynamic stall control

by leading edge vortex generators", J. Am. Helicopter Soc. 53(1), pp. 26-36 (2008)

[2] Martin, P., Wilson, J., Berry, J., Wong, T., Moulton, M., McVeigh, M., "Passive Control of Compressible Dynamic Stall", AIAA Paper 2008-7506, 2008.

[3] LePape, A., Costes, M., Joubert, G., David, F., Deluc, J.-M., "Experimental Study of Dynamic Stall Control Using Deployable Leading-Edge Vortex Generators", AIAA Journal, Vol. 50, No. 10 (2012), pp. 2135-2145.

[4] Gardner, A.D., Richter K., Mai, H., Neuhaus, D., "Experimental control of compressible OA209 dynamic stall by air jets", 38th ERF, Amsterdam, 4-6 Sept, 2012.

[5] Weaver, D., McAlister, K.W., Tso, J., "Control of VR7 Dynamic stall by strong steady blowing", Journal of Aircraft, Vol. 41, No. 6, 2004.

[6] Kaufmann, K., Gardner, A.D., Richter, K., "Numerical investigations of a back-flow flap for dynamic stall control", STAB 2012, Stuttgart, 6-7 November, 2012.

[7] Meyer, R.K.J., "Experimentelle Untersuchungen von Rückstromklappen auf Tragflügeln zur Beeinflussung von Strömungsablösungen", Dissertation Technische Universität Berlin, Mensch-und-Buch-Verlag, 2000.

[8] Höfinger, M., "Rotorblatt mit integrierter passiver Oberflächenklappe", Deutsches Patent DE 10 2010 041 111 A1, 22.03.2012.

[9] Gallot, J., Vingut, G., De Paul, M. V., Thibert, J., "Blade profile for rotary wing of an aircraft", United States Patent 4325675,(20.4.1982).

[10] Mulleners, K., Raffel, M., "The onset of dynamic stall revisited", Experiments in Fluids, Vol. 52, (3), pp 779-793, 2012. DOI 10.1007/s00348-011-1118-y

[11] Gardner, A.D., Richter, K., Rosemann, H., "Numerical investigation of air jets for dynamic stall control on the OA209 airfoil", CEAS Aeronautical Journal, Volume 1, Issue 1, Page 69-82, 2011. DOI 10.1007/s13272-011-0002-z

[12] Schwamborn, D., Gardner, A.D., von Geyr, H., Krumbein, A., Lüdeke, H., Stürmer, A. "Development of the TAU-Code for aerospace applications" *50th NAL INCAST (International Conference on Aerospace Science and Technology)*, Bangalore, India, 2008.

[13] Richter, K., Le Pape, A., Knopp, T., Costes, M., Gleize, V., Gardner, A.D., "Improved Two-Dimensional Dynamic Stall Prediction with Structured and Hybrid Numerical Methods", *AHS Journal*, Volume 56, 2011.

[14] Schwarz, T., "The Overlapping Grid Technique for the Time Accurate Simulation of Rotorcraft Flows", In: 31st ERF, Florence, Italy, 13. - 15. September 2005.

[15] Spalart, P. R., Allmaras, S. R., "A one-equation turbulence model for aerodynamic flows", AIAA Paper 92-0439, AIAA 30th Aerospace Sciences Meeting and Exhibit, Reno, Jan 6-9,1992.

[16] Kaufmann, K., "Numerische Untersuchung einer Rückstromklappe zur Dynamic Stall-Kontrolle", Diplomarbeit, Uni. Stuttgart IAG, 2012.

[17] Gardner, A.D., Richter K., "Influence of rotation on dynamic stall", American Helicopter Society 68th Annual Forum, Fort Worth, Texas, May 1-3, 2012.

[18] Wierach, P., "Nano-Micro-Macro", Adaptive, Tolerant and Efficient Composite Structures, Research in Aerospace, Wiedemann,M. and Sinapius,M. (eds), Springer-Verlag Berlin Heidelberg 2012. DOI 10.1007/978-3-642-29190-6_2, pp. 17-28

[19] Wierach, P., Riemenschneider, J., Opitz, S., Hoffmann, F., "Experimental Investigation of an Active Twist Model Rotor Blade Under Centrifugal Loads", Adaptive, Tolerant and Efficient Composite Structures, Research in Aerospace, Wiedemann, M. and Sinapius, M. (eds), Springer-Verlag Berlin Heidelberg 2012. DOI 10.1007/978-3-642-29190-6_32, pp. 391-407

[20] Wierach ,P., "Low Profile Piezo Actuators Based on Multilayer Technology", 17th International Conference on Adaptive Systems and Structures, 2006-10-16 - 2006-10-19, Taipei, Taiwan.

[21] Grote, K. H., Feldhusen, J. (eds), "Dubbel: Taschenbuch für den Maschinenbau", 23rd edition, Springer-Verlag Berlin Heidelberg 2012

[22] Opitz, S., Riemenschneider, J., Hoffmann, F., Schneider, O., "Measurement of the dynamic tip twist angles of an Active Twist model scale rotor blade", 36th European Rotorcraft Forum, 07.-09. September 2010, Paris, France

[23] Wierach,P.,"Piezocomposite Transducers for Adaptive Structures", Adaptive, Tolerant and Efficient Composite Structures, Research in Aerospace, Wiedemann, M. and Sinapius, M. (eds), Springer-Verlag Berlin Heidelberg 2012. DOI 10.1007/978-3-642-29190-6_3, pp. 29-47

[24] Algermissen, S., Keimer, R., Rose, M., Straubel, M., Sinapius, M., Monner, H.P., "Smart-Structures Technology for Parallel Robots", Journal of Intelligent and Robotic Systems, Vol. 63, pp. 547-574. Springer Verlag 2011. DOI 10.1007/s10846-010-9522-8. ISSN 0921-0296.